Designing a Bernal Spiral from Patchy Colloids

John W. R. Morgan,[†] Dwaipayan Chakrabarti,[†,‡] Nicolas Dorsaz,[†] and David J. Wales[†,*]

[†]University Chemical Laboratories, Lensfield Road, Cambridge CB2 1EW, United Kingdom and [‡]Department of Chemistry, Indian Institute of Technology Delhi, Hauz Khas, New Delhi 110 016, India

ABSTRACT A model potential for colloidal building blocks is defined with two different types of attractive surface sites, described as complementary patches and antipatches. A Bernal spiral is identified as the global minimum for clusters with appropriate arrangements of three patch−antipatch pairs. We further derive a minimalist design rule with only one patch and antipatch, which also produces a Bernal spiral. Monte Carlo simulations of these patchy colloidal building blocks in the bulk are generally found to corroborate the global optimization results.

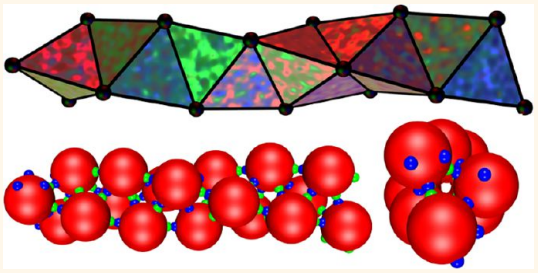

KEYWORDS: Bernal spiral · patchy colloids · self-assembly · patch−antipatch · anisotropic interactions · global optimization

The synthesis of colloidal particles is important in such areas as paints, hygiene products, drug delivery, and nanotechnology. Their diversity makes such particles attractive candidates for the design of self-assembling nanodevices.[1] Much recent synthetic effort has been spent on moving beyond simple spherical colloids to anisotropic particles of various shapes.[2−4] Colloidal particles have also been synthesized with "sticky patches" on their surfaces, which interact with patches on other particles.[2,4] This functionality suggests the possibility for self-assembly of complex structures *via* a bottom-up approach, without the need for the detailed control required in a top-down method. Self-assembly is governed by the interactions between the building blocks, so in principle, rational design of building blocks, tuning their mutual interactions, can lead to systems that self-assemble into specific target structures.[3]

Simulation of self-assembling systems is a useful tool in guiding the synthesis of particles, which can suggest interesting synthetic targets.[5] Rational design of building blocks for self-assembly is greatly facilitated if the final structure can be predicted as a function of the building block parameters. The corresponding energy landscape contains all the information necessary for such a prediction, both in terms of the energetically favorable minima, and the pathways between them, which determine the structures that can easily be assembled.[6−8] The simplest model of colloidal particles involves hard spheres with a short-range square-well attraction,[9] but other potentials such as the Lennard-Jones and Morse forms have also been considered.[10−13]

Anisotropic building blocks open up rich avenues for sophisticated self-assembly into a variety of target structures.[3,14] Isotropic models are not sufficient for describing these building blocks, and representations with directional patches have been considered.[15,16] For example, Wilber, Doye, and Louis used a model with Gaussian patches to study the self-assembly of particles designed to form the five platonic solids.[17] They concluded that targets with triangular faces are the easiest to assemble.

An assembly of particles with a diamond-like crystal structure has been suggested as a synthetic target due to the potentially interesting photonic properties,[18,19] and numerical studies of patchy particles have been carried out to investigate whether they will crystallize to form this lattice.[20] Creating a patchy particle that will assemble into this crystal has so far had limited success, due to the presence of frustration[21] in the energy landscape.[22] A refinement of the patchy model that involves two types of patches ("patches" and "antipatches") has been suggested in the context of protein crystallization,[23,24] and by Wilber and coworkers as a route to more complicated self-assembly targets.[17] Here an antipatch is a

* Address correspondence to dw34@cam.ac.uk.

Received for review October 9, 2012 and accepted January 24, 2013.

Published online January 24, 2013
10.1021/nn304677t

second type of patch that interacts with patches, but not with other antipatches. Doye *et al*. have proposed a binary mixture of oppositely charged patchy colloids to achieve a similar effect.[22]

The present contribution focuses on the Bernal spiral, a three-stranded helix composed of a chain of face-sharing tetrahedra,[25] as the target structure. Although edge-sharing and corner-sharing chains of tetrahedra are common, for example in silicate minerals,[26,27] extended chains of face-sharing tetrahedra are much rarer.[28] The spiral, first proposed by Bernal,[25] has been investigated in connection with order in supercooled fluids.[29,30] The feasibility of assembling this structure at a molecular level has also been investigated.[28] Direct imaging of colloid gels by confocal microscopy has revealed the presence of a network of short connected Bernal spirals,[31,32] while triple helices formed from face-sharing tetrahedra have been identified for assemblies of Janus spheres.[33] Such short spiral strands have also appeared in computational models of colloidal clusters involving only isotropic interactions[34,35] and have recently been identified in a bimetallic cluster.[36]

Here we define a potential for patchy colloids involving an isotropic component, describing the interaction between spherical cores, and an anisotropic component governed by two types of complementary patches, in the spirit of the patch–antipatch (PAP) framework recently introduced by Dorsaz *et al*.[24] A key feature of our representation is that the potential is continuous, unlike most models for patchy colloids. This feature makes the representation suitable for structure prediction by global optimization techniques that rely upon geometry optimization, as well as molecular dynamics simulations. Using basin-hopping global optimization, the model is investigated for different realizations of patch–antipatch interactions, which enables us to design a minimal representation of the building blocks that supports a Bernal spiral. Subsequent Monte Carlo simulations are generally found to corroborate the global optimization results.

RESULTS AND DISCUSSION

Patch–Antipatch Arrangement. A Bernal spiral can be described as a stack of face-sharing regular tetrahedra. If particles are placed at the vertices of each tetrahedron, a three-stranded helix results, with each particle having six nearest neighbors, except those at the ends. A PAP arrangement was designed so that there is a patch or antipatch pointing at each of the nearest neighbors. The three sticky spots pointing one way along the helix, in the direction taken to be the positive *z*-direction, were assigned as patches, while the three pointing in the negative *z*-direction were assigned as antipatches.

The particles can be considered to lie on the surface of a cylinder along the *z*-axis with radius $r = 3\sqrt{3}/10$, where the *z* offset between each particle is $h = 1/\sqrt{10}$.

TABLE 1. The Patch and Antipatch Directions for a Right-Handed Bernal Spiral

particle number	particle position (*xyz*)			patch type (label)	patch direction (*xyz*)		
−3	0.423	−0.301	−0.949	p' (3′)	−0.096	−0.301	−0.949
−2	−0.058	0.516	−0.633	p' (2′)	−0.577	0.516	−0.633
−1	−0.346	−0.387	−0.316	p' (1′)	−0.866	−0.387	−0.316
0	0.520	0	0				
1	−0.346	0.387	0.316	p (1)	−0.866	0.387	0.316
2	−0.058	−0.516	0.633	p (2)	−0.577	−0.516	0.633
3	0.423	0.301	0.949	p (3)	−0.096	0.301	0.949

The angular offset around the *z*-axis between two successive patches is $\theta = \arccos(-2/3) \approx 131.8°$. It is interesting to note that θ is irrational, meaning that no two particles in a spiral will ever have identical *x* and *y* coordinates. With these definitions, the coordinates of the *n*th particle in the helix can be written as

$$\mathbf{x}_0 = (r, 0, 0), \qquad \mathbf{x}_n = (r\cos n\theta, r\sin n\theta, nh) \quad (1)$$

The structure is actually chiral, with right-handed and left-handed structures; eq 1 gives the right-handed spiral. The left-handed spiral can be obtained by inverting the sign of the *y* coordinate in eq 1, but only the right-handed spiral is considered explicitly below unless otherwise specified. If eq 1 is used to calculate the positions of seven consecutive particles ($n = -3$ to $+3$), the positions of six particles relative to that of particle zero provide the directions in which the patches and antipatches on the latter particle should point. These direction vectors are collected in Table 1.

Optimization of Parameters. Initially, global optimization runs were carried out with small clusters of 12 and 18 particles (four per strand and six per strand, respectively) without periodic boundary conditions to find a set of PAP potential parameters for which a favorable Bernal spiral structure could be quickly identified. Given the tailor-made arrangement of patches and antipatches, it is not surprising that the Bernal spiral was indeed found to be the global minimum for a wide range of parameter space with three pairs of patches and antipatches. Figure 1 shows plots of the potential and its different components for an ideal PAP alignment with a representative set of parameters.

Finding the global minimum quickly does not necessarily mean that the structure would self-assemble easily, because the physically relevant dynamics can be trapped by frustration,[6,17] which can be overcome by the large basin-hopping (BH) steps during global optimization. However, being able to find the spiral quickly is a good starting point. It was found that lower values for *s*, a lower $\cos\delta$, and a higher ε all favored finding the spiral quickly (see Methods section for definitions of these parameters). These results can be understood in terms of the underlying energy landscape: changing the parameters as stated increases the width and/or depth of the basin of the spiral, making it more likely that a BH step

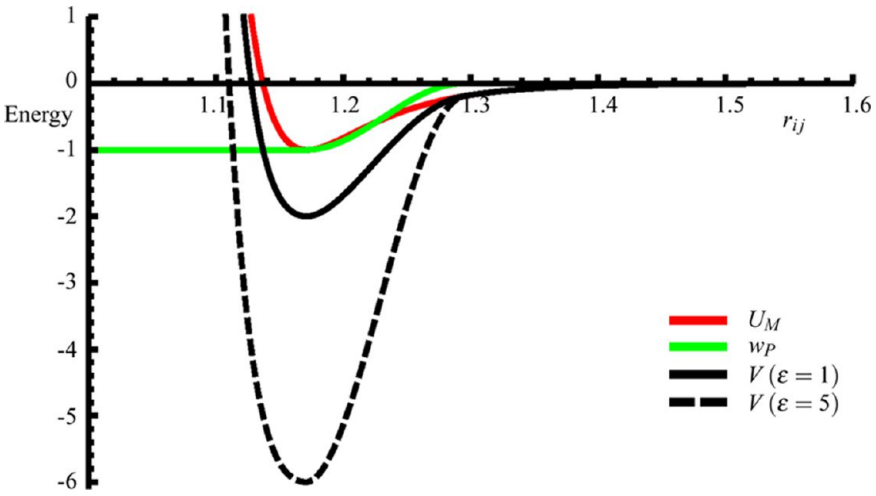

Figure 1. Plots of V, U_M, and w_P for two values of ε with $\alpha = 40$ and $s = 8$. These plots correspond to a patch and an antipatch pointing directly at each other.

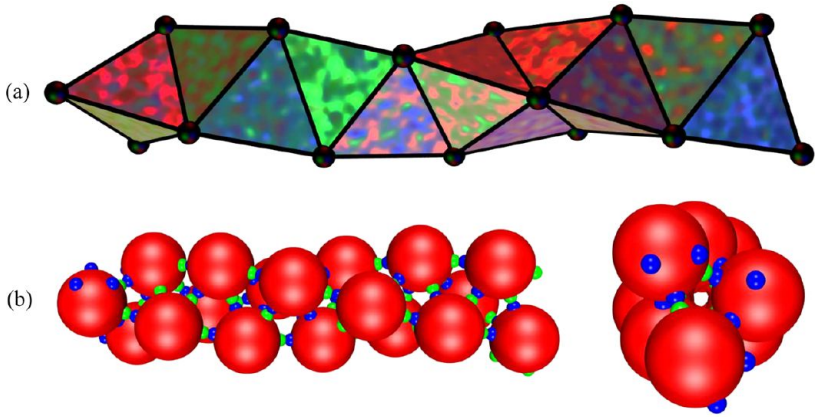

Figure 2. Alternative views of a Bernal spiral consisting of 18 particles. The particles are represented by the black spheres at the tetrahedron vertices in the space-filling representation in (a). The texture and coloring of the faces were chosen to render the packing as clear as possible. The structure is chiral; this is the right-handed structure. In the side and top views in part (b) larger spheres in red depict the particle cores, while smaller spheres represent patches (blue) and antipatches (green).

enters the funnel leading to the global minimum, and then does not easily escape. The parameters chosen for further study were $\alpha = 40$, $s = 8$, $\cos\delta = 0.75$, and $\varepsilon = 5$, which usually meant that the Bernal spiral was found within 10^4 BH steps. The 18-particle spiral, which is the global minimum, is shown in Figure 2.

Variation of Parameters. Having established a set of parameters for the PAP potential that produced a Bernal spiral as the global minimum, various modifications were considered to establish design principles that could be followed in experimental fabrication. First, the patch width was analyzed. It is intuitive that the Bernal spiral will also be the global minimum at any narrower patch width ($\cos\delta > 0.75$), as a narrower patch will not affect the energy of the spiral so long as a PAP pair can be aligned. However, very narrow patches are likely to make it difficult for the patch−antipatch pairs to locate each other, and thus lead to slow assembly. The same is not true for wider patches, as at some point, when patches start to overlap significantly, there is the possibility of one patch pointing between two antipatches (or *vice versa*) and having a favorable interaction with both. We found this situation for $\cos\delta \leq 0.65$, where the disordered structure, shown in Figure 3a, becomes the global minimum.

Increasing the value of ε produces similar effects to increasing the value of $\cos\delta$. However, increasing ε will change the shape of the landscape, deepening the basins of frustrated local minima as well as the global minimum. Beyond a certain point, raising the value of ε is expected to increase frustration and therefore hinder self-assembly. With $\varepsilon = 0$ (no PAP attraction) the global minimum is a fragment of a hexagonal close-packed lattice, as shown in Figure 3b. This structure is not the same as the global minimum of the standard 12−6 Lennard-Jones potential[37] due to the shorter range of the 46−23 Mie potential employed here. A shorter range destabilizes strained geometries, whose nearest-neighbor contact distances deviate more from the optimal value, and favors close-packed structures.[38,39]

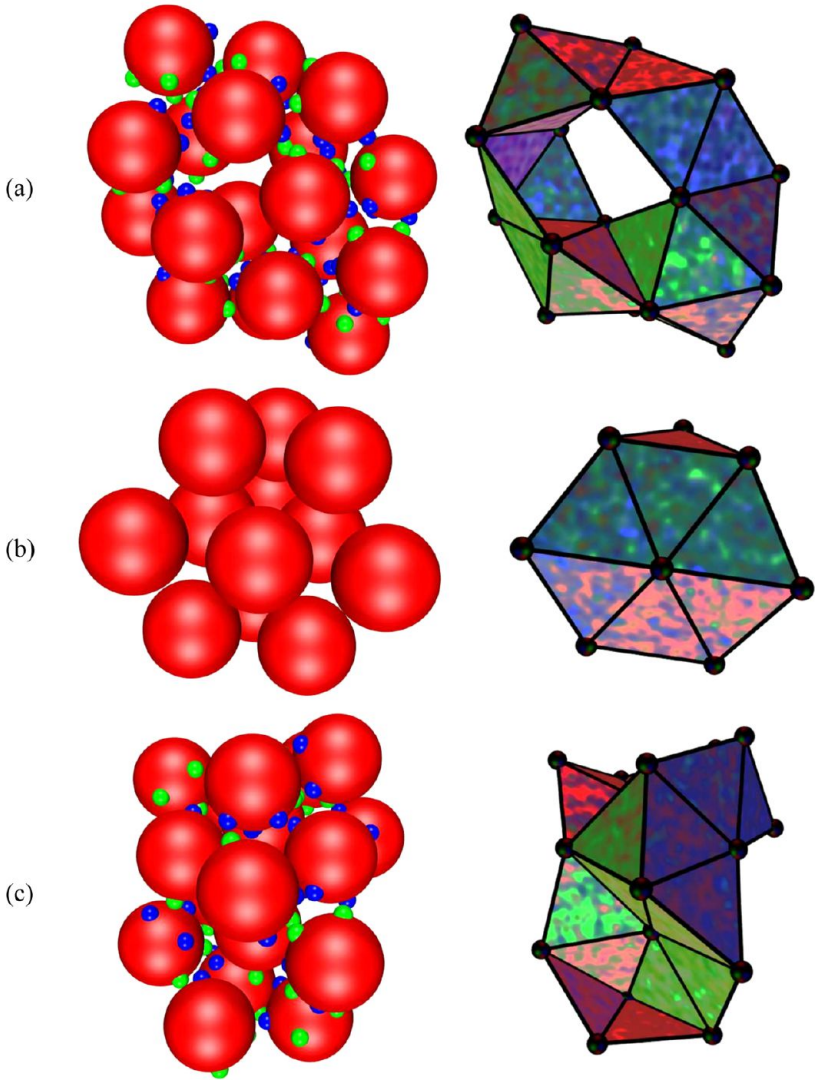

Figure 3. Alternative representations of the global minima of clusters obtained for different sets of parameters. (a) For an 18-particle cluster with $\cos\delta = 0.65$. Unlike Figure 2, some of the patches point between the antipatches on other particles, indicating interactions between multiple patches and antipatches for some pairs of particles. This structure is 16% lower in energy than the Bernal spiral with $\cos\delta = 0.65$. (b) For a 12-particle cluster with $\varepsilon = 0$. There is no PAP attraction, only the isotropic 46−23 Mie potential. (c) For an 18-particle cluster with patch directions perturbed by up to 0.25 radians. As in representation (a) some of the patches point between the antipatches on other particles, indicating multiple interactions between some pairs.

The minimum in Figure 3b has an energy 10% lower than predicted for a Bernal spiral constituted from these particles. In fact, the Bernal spiral is the global minimum for values above $\varepsilon \simeq 1$. It therefore follows that attempts to synthesize patchy building blocks directed at self-assembly of a Bernal spiral should include patches with an attraction at least as strong as the isotropic attraction between particles.

Since experimental syntheses are unlikely to produce patches with perfect geometrical distributions, random perturbations were made to the patch orientations, to estimate the angular tolerance of the global minimum. To perturb each patch, a normalized vector was generated from three uniformly distributed random numbers between 0 and 1. The cross product of this vector with the patch orientation vector was taken, to produce a normalized vector with uniformly random orientation within the plane perpendicular to the patch vector. The patch vector was rotated about the perpendicular vector by an angle uniformly chosen from the range $-\theta$ to $+\theta$, where θ (in radians) is the specified maximum rotation. Ten sets of patch directions were generated for each value of θ, and the global minima were located. For $\theta \leq 0.24$ small changes to the energy, of order 1%, were found, but the Bernal spiral structure was preserved. For $\theta \geq 0.25$ disordered structures, such as the one shown in Figure 3c, were formed. The structure in Figure 3c is 10% lower in energy than the unperturbed minimum. As for changes in the patch width, $\theta = 0.25$ is the point at which it becomes possible for significant interactions between multiple patches and antipatches on one pair of particles to occur.

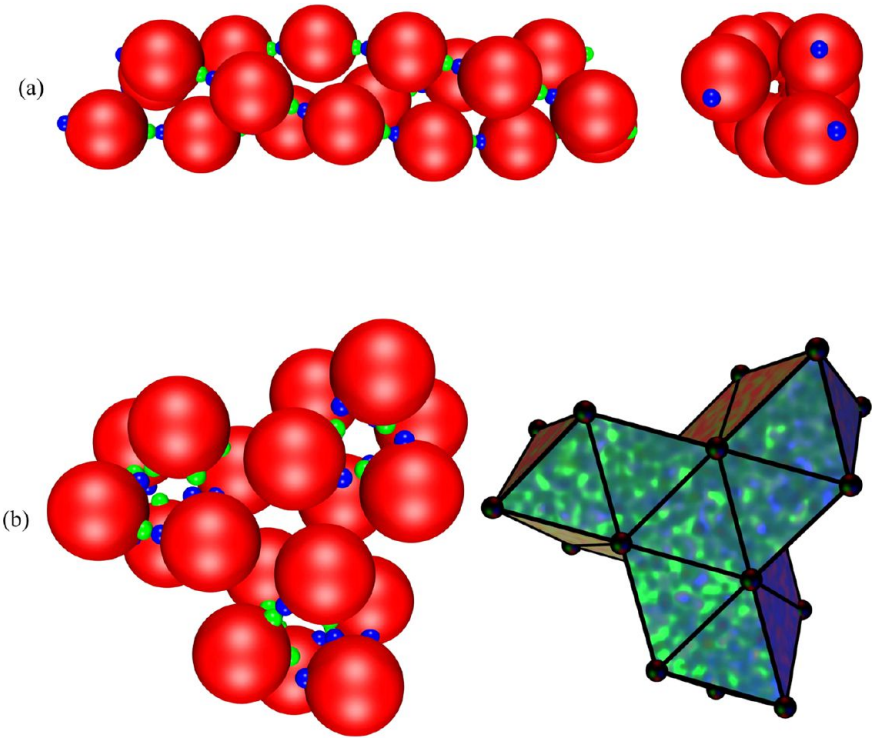

Figure 4. (a) Side and top views of the global minimum for 18 particles, with only the PAP pair (3,3′). (b) Alternative representations of the global minimum for 18 particles, without the PAP pair (3,3′). This structure is composed of three octahedra and is 4% lower in energy than the Bernal spiral formed from the same building blocks.

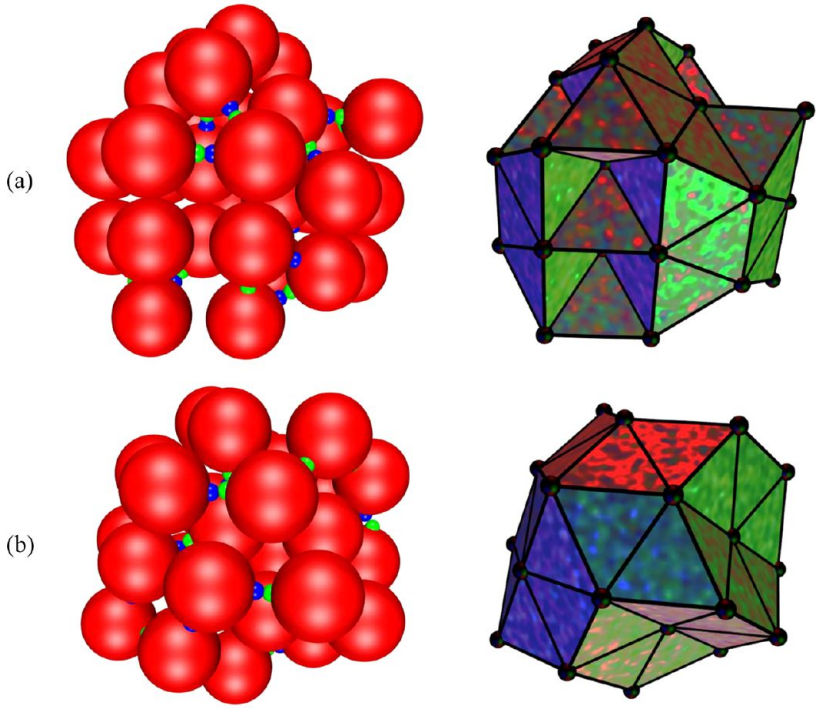

Figure 5. The global minima for 30 particles and periodic boundary conditions with: (a) the PAP pair (1,1′). The energy is 5.4% lower than predicted for the Bernal spiral. (b) the PAP pair (2,2′). The energy is 3.3% lower than for the Bernal spiral.

Removal of Patches. It is important to determine which patches are actually necessary for the assembly of the Bernal spiral and which are superfluous, so that a minimalist design rule can be identified to guide experimental synthesis of building blocks. To this end, pairs of patches and antipatches were removed and the global minimum was located using basin-hopping. Our results suggest that only the (3,3′) PAP pair (see Table 1)

is necessary. Figure 4 shows a Bernal spiral formed with only these patches. Hence we predict formation of a Bernal spiral with colloidal building blocks having only one patch and antipatch at ~169° to each other. It is worthwhile to note that with only one PAP pair, the building block is achiral and enantiomeric right- and left-handed Bernal spirals are the global minima. Figure 4 also shows the global minimum for 18 particles without the (3,3′) PAP pair, but with the other patches and antipatches. This structure is composed of three octahedra, and arises due to the fairly wide patches being used, illustrating the diverse variety of structures achievable through a judicious choice of patch and antipatch distributions.

Periodic Boundary Conditions. For a Bernal spiral of finite length, some of the patches and antipatches at the ends of the strands have no interactions (six at each end) and this will affect the stability of the structure. We therefore considered the building blocks under periodic boundary conditions. Due to the short-range nature of the potential, the minimum image convention was followed to reduce the computational burden. This choice means that each particle interacts with at most one image of every other particle, simplifying the calculation.

The irrational θ means that no two particles will ever lie precisely on top of each other, even in a very long spiral, which implies that any representation of the Bernal spiral as a repeating unit must introduce some perturbation of the structure. It was found that with vertex zero chosen as defined in Table 1, vertex 30 was at (0.517, −0.052, 9.489). Vertex 30 was deemed sufficiently close in x and y to be treated as a repeat of vertex zero, so periodic structures were considered with 30 particles. The full 30-particle periodic spiral (not shown here) has an energy only 0.05% higher than expected for 90 perfectly aligned PAP interactions.

The removal of patches was also analyzed using periodic boundary conditions. Again it was found that with only the (3,3′) PAP pair, the Bernal spiral was the global minimum. When PAP pairs (1,1′) and (2,2′) were used, the spiral remained the global minimum, with a cluster of five octahedra 2.4% higher in energy. This result arises from the absence of noninteracting ends of the spiral, which lowers its energy relative to the octahedral cluster. With PAP pairs (1,1′) and (3,3′), and with pairs (2,2′) and (3,3′), the Bernal spiral was also the global minimum. For the single PAP pair (1,1′) a cluster was formed, which was too small to interact with its periodic images, containing triangles fulfilling all the PAP interactions, but with more isotropic interactions than the spiral. A similar cluster formed for the PAP pair (2,2′), but with larger loops of particles, due to the larger angle between patches (Figure 5).

We also considered compressing the geometry by reducing the size of the box, while maintaining the number of particles, in order to create the sort of defects visible in confocal microscope images.[31] The defect structures include bent Bernal spirals, and spiral fragments that join at an angle. Figure 6 shows structures obtained from a cubic box of edge length 10.5, 9.5, and 8.5 (compared with 11.1 for the perfect structure). The geometry for 10.5 shows that a small amount of compression can be accommodated by supercoiling the helix, whereas for a box length of 9.5, the Bernal spiral is broken. The structure with a box length of 8.5 exhibits a sawtooth morphology. All these structures are only a little higher in energy than the uncompressed perfect Bernal spiral (not shown). The increase for the 10.5 structure is due to imperfect alignment of the patches. For the other structures a few of the patches and antipatches have unsatisfied contacts, as indicated by green and blue spheres without a contact.

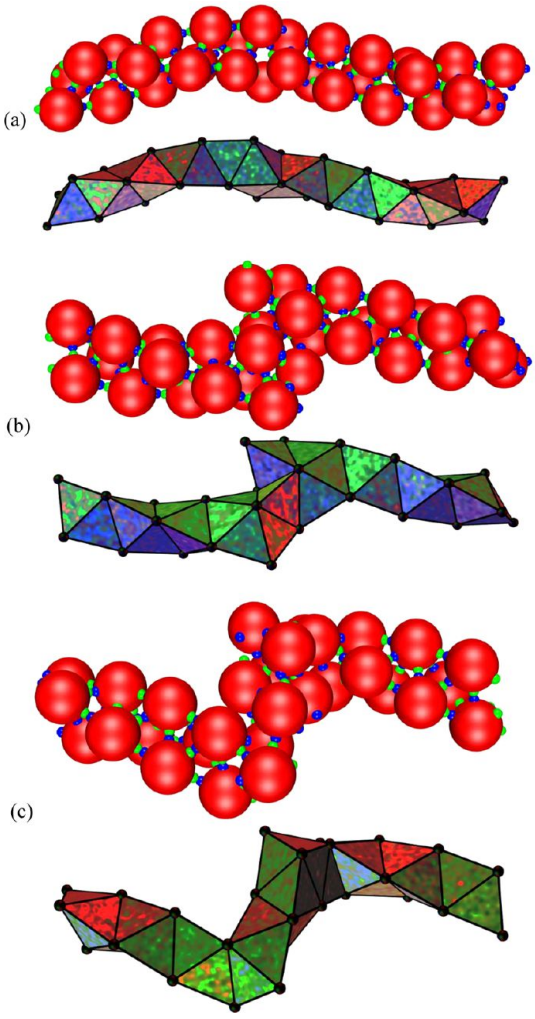

Figure 6. Alternative representations of the global minima for 30 particles and periodic boundary conditions with decreasing box size. (a) With a box length of 10.5, we see supercoiling of the helix. (b) For a box length of 9.5, the spiral is broken. (c) With box length 8.5, the global minimum exhibits two breaks, forming a sawtooth pattern. These three structures are higher in energy by 3.5%, 5.7%, and 6.4%, respectively, compared to the Bernal spiral obtained with a box length of 11.1 (not shown).

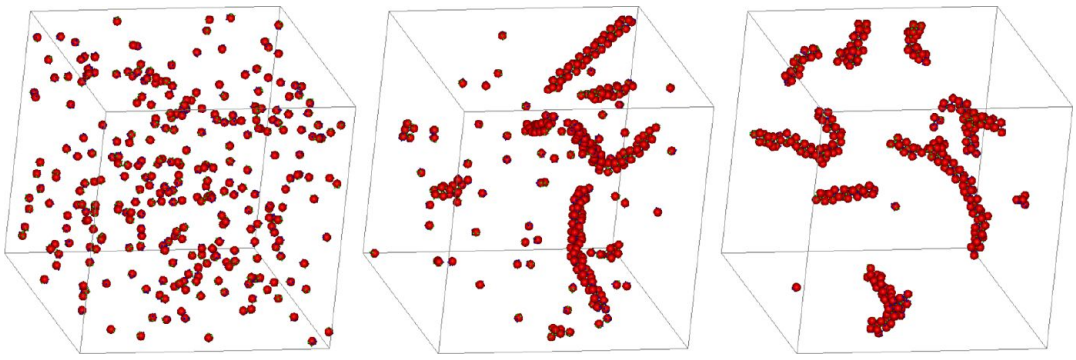

Figure 7. Snapshots of configurations obtained from Monte Carlo simulations of patchy colloids with all three pairs of patches and antipatches at three temperatures (T = 0.20, 0.18, 0.10 from left to right) in the absence of isotropic attraction between the particles (ε_{iso} = 0). Bernal spirals in equilibrium with a low density liquid are obtained on decreasing the temperature below T = 0.20. For temperatures below about 0.15 the system is arrested in many short spirals.

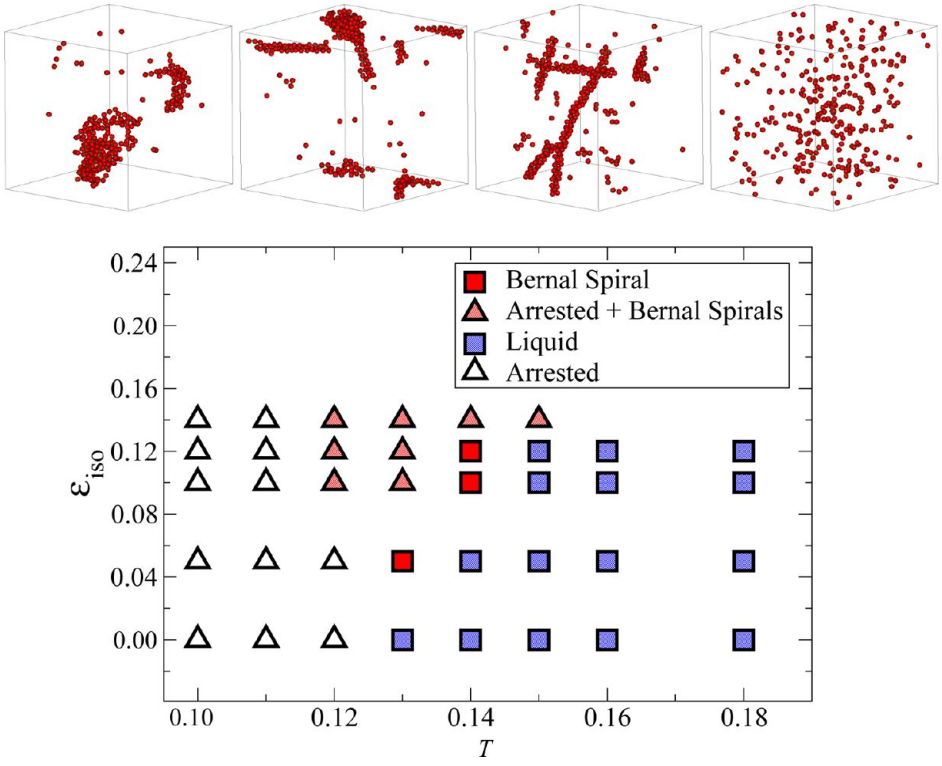

Figure 8. Phase behavior of patchy colloids with the PAP pairs (2,2′) and (3,3′) in the temperature−ε_{iso} plane. Snapshots of configurations corresponding to different states are also shown; from right to left, a liquid state, a state with predominantly Bernal spiral structures, a somewhat arrested state with some Bernal spiral structures, and a completely arrested state. The phase diagram is based on the final configurations of our Monte Carlo runs.

Monte Carlo Simulations. To test whether the Bernal spirals obtained from global optimization can indeed be self-assembled under thermal conditions we performed Monte Carlo simulations of the bulk. To speed up the computation and reduce the parameter space we employed the generalized version of the Kern−Frenkel potential,[15] recently introduced by Dorsaz *et al.*,[24] to describe the PAP interaction, while the isotropic component was represented by a hard sphere interaction with an attractive square-well of strength ε_{iso}. The range of both the isotropic and the PAP interactions was set to λ' = 1.24d, where d is the hard sphere diameter. This discontinuous potential is very close to the continuous form employed in the global optimization searches. The parameter controlling patch width was set to 0.94 to ensure that a patch can only interact favorably with a single complementary patch for the chosen range of the square-well potential. The key parameters that we varied are ε_{iso} and the temperature T, both expressed in units of the PAP interaction, ε_{pap}. All the Monte Carlo simulations were performed at a packing fraction of $\phi = \pi/6\rho d^3$ = 0.0058 and with N = 300 particles. A rather dilute system was chosen to reduce the possibility of the system getting into kinetic traps.

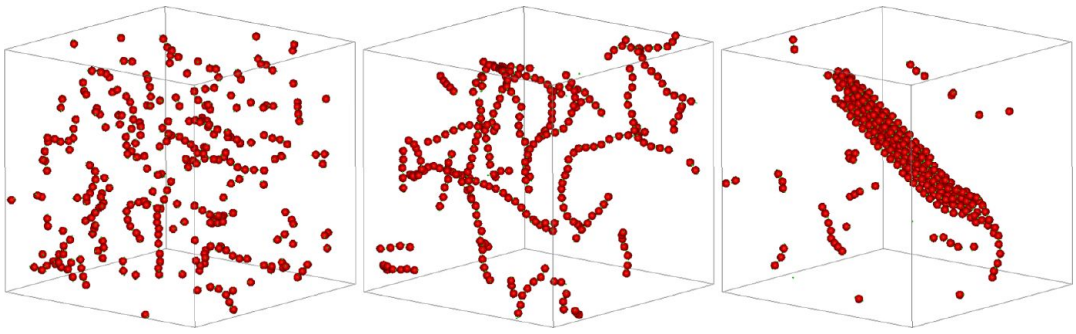

Figure 9. Snapshots of configurations obtained from Monte Carlo simulations of patchy colloids with only the PAP pair (3,3′), showing chains of particles and fiber-like structures. From left to right, (T,ε_{iso}) = (0.09, 0.00), (0.07, 0.05) and (0.08, 0.10).

We first considered a system of patchy colloids with three pairs of patches and antipatches, as in Table 1. We found that the isotropic attraction between the particles was not necessary for the Bernal spiral to be observed. For $\varepsilon_{iso} = 0$, the system assembles into Bernal spirals in equilibrium with a low density liquid at intermediate temperatures. At high temperatures it forms a liquid state and at low temperatures we observed an arrested state composed of spirals (Figure 7). Next, we show the phase behavior in the $T-\varepsilon_{iso}$ plane in Figure 8 for the patchy colloids with the PAP pair (1,1′) removed. For a purely patchy attraction between the particles (*i.e.*, $\varepsilon_{iso} = 0$) we did not observe the assembly of Bernal spirals in our Monte Carlo simulations for the discrete set of temperatures investigated. The system passes directly from a liquid state at $T = 0.13$ to a condensed state at $T = 0.12$. When the isotropic square-well attraction between the particles was turned on at $\varepsilon_{iso} = 0.05$, a narrow regime was found at intermediate temperatures where equilibrium Bernal spirals formed. For slightly larger ε_{iso}, the spirals also nucleated, but out of dense liquid droplets in what appears to be an interesting two-step nucleation process. At slightly lower temperatures [such as state point (0.12,0.12)] Bernal spirals formed less easily out of the condensed (almost arrested) liquid and nucleation was incomplete on the simulation time scale. Above $\varepsilon_{iso} = 0.15$, condensation due to the isotropic part of the interaction dominated over directional PAP interaction, preventing the formation of spirals.

Finally, we performed a similar study with only the PAP pair (3,3′) on each particle. We found more complex behavior, encompassing liquid and condensed phases and an interesting phase, where chains of particles formed (low T and small ε_{iso}) and assembled into long compact fibers (made of more than three chains) upon increasing ε_{iso} (Figure 9). However, we have not yet been able to tune the temperature and ε_{iso} to observe the Bernal spiral structure in this case. Given the sensitivity to small changes of T or ε_{iso}, it is possible that spirals may form for different combinations of parameters or different packing fractions, or that longer simulations are required.

CONCLUSIONS

The PAP potential employed in the present work provides a powerful model for investigating systems of monodisperse patchy colloidal particles, which are of increasing interest as synthetic techniques advance. Given the tailored spatial arrangement of three pairs of patches and antipatches in the six-patch building blocks considered here, it is not surprising that we observed Bernal spirals as the global minima for finite-size systems initially. The key finding of the present work is a minimalist design rule that we derive by systematic removal of the patches. A patch−antipatch pair offset slightly (∼10°) from the directly opposite spatial arrangement is found to be sufficient for the ground state structure to be a Bernal spiral. The present work not only offers a minimalist design rule that is a realistic target for state-of-the-art experimental fabrication, it also describes a rational approach to derive this rule. Another critical element of the design is that the directional patch−antipatch attraction must be stronger than the isotropic interaction. Our strategy is found to be quite robust to imperfection in the spatial arrangement of the patch−antipatch pairs. This feature makes the building blocks attractive for experimental fabrication to realize target structures *via* self-assembly.[40] Compressed spirals exhibit supercoiling or breaks, which resemble structures seen in confocal microscopy.

The observation of triple helices with Janus spheres in recent experimental work and in a related model system,[33] where directionality of interactions plays a crucial role, is clearly relevant to the present work. Bernal spirals, alternatively called Boerdijk−Coxeter helices, emerged in the experiments with Janus spheres through kinetics, while we have derived design principles for thermodynamically favorable Bernal spirals with patchy interactions. It is interesting to note that our two-patch building blocks with complementary patch and antipatch are similar in spirit to Janus particles, especially for wider patch widths.

The PAP potential is also likely to be useful for investigating protein crystallization. As the potential has no inherent length scale, tuning the parameters for roughly spherical proteins should be possible. Patch

configurations could be designed based on crystal contacts in known structures, or on the nature of surface residues. Having such a simple potential that could usefully mimic protein crystallization would be a significant asset in the ongoing investigations into this process.[32,41,42]

METHODS

The Model. The patch−antipatch potential considered here models patchy colloids in terms of rigid building blocks consisting of a spherical core with decorated patches of two types, which are called "patches" and "antipatches" to distinguish them. The potential is defined by an isotropic component describing the interaction between the spherical cores, and an anisotropic component describing the directional interaction between patches, p, and antipatches, p'. Patches have an attractive interaction with antipatches, but do not interact with other patches; nor do antipatches interact with other antipatches. The PAP interaction includes a short-ranged spherically symmetric potential modulated by a function of the relative orientations of the PAP pair, and hence is anisotropic overall. Only pairwise interactions are considered, and the pair potential can be written as

$$V(\mathbf{r}_{ij}, \mathbf{\Omega}_i, \mathbf{\Omega}_j) = U_{\mathrm{M}}(r_{ij}) + U_\theta(\mathbf{r}_{ij}, \mathbf{\Omega}_i, \mathbf{\Omega}_j) w_{\mathrm{P}}(r_{ij}) \quad (2)$$

where $\mathbf{r}_{ij} = \mathbf{r}_j - \mathbf{r}_i$ is the vector displacement of rigid body j relative to i, r_{ij} is the distance between bodies i and j, and $\mathbf{\Omega}_i$ defines the orientation of body i. The isotropic component, U_{M}, is a 46−23 Mie potential.[43] This form was chosen to match closely what was proposed by ten Wolde and Frenkel,[44] but without the hard-core repulsion:

$$U_{\mathrm{M}}(r_{ij}) = 4\left[\left(\frac{\sigma}{r_{ij}}\right)^{46} - \left(\frac{\sigma}{r_{ij}}\right)^{23}\right], \qquad \sigma = \sqrt{1 + \frac{1}{\alpha^{1/3}}} \quad (3)$$

The parameter α can be used to control the range of the isotropic potential relative to the patch−antipatch interaction. The distance dependence of the PAP attraction is governed by the function w_{P}:

$$w_{\mathrm{P}}(r_{ij}) = \begin{cases} -1, & \text{if } (r_{ij} - \lambda) < 0 \\ -\frac{1}{2}[1 + \cos(\pi(r_{ij} - \lambda)s)], & \text{if } 0 \le (r_{ij} - \lambda) \le s^{-1} \\ 0, & \text{if } (r_{ij} - \lambda) > s^{-1} \end{cases} \quad (4)$$

$$\lambda = \sqrt{1 + \left(\frac{2}{\alpha}\right)^{1/3}} \quad (5)$$

where λ is the largest separation at which the attraction is at its strongest and the parameter s controls the range over which the attraction decreases to zero. A larger value of s gives a steeper slope. The angular dependence of the PAP attraction is described by U_θ:

$$U_\theta(\mathbf{r}_{ij}, \mathbf{\Omega}_i, \mathbf{\Omega}_j) = \varepsilon_{\mathbf{p}_i, \mathbf{p}_j} \frac{1}{4}[1 + \Phi(\mathbf{r}_{ij}, \mathbf{\Omega}_i, \mathbf{p}_i)][1 + \Phi(\mathbf{r}_{ji}, \mathbf{\Omega}_j, \mathbf{p}_j)] \quad (6)$$

$$\Phi(\mathbf{r}_{ij}, \mathbf{\Omega}_i, \mathbf{p}_i) = \begin{cases} -1, & \cos\theta_{ijp_i} < \cos\delta \\ -\cos\left(\frac{\pi[\cos\theta_{ijp_i} - \cos\delta]}{1 - \cos\delta}\right), & \cos\theta_{ijp_i} \ge \cos\delta \end{cases} \quad (7)$$

The maximum strength of the PAP interaction compared to the isotropic potential is controlled by $\varepsilon_{\mathbf{p}_i\mathbf{p}_{i'}}$ which is nonzero only if the two patches are of opposite type. $\mathbf{p}_i$ is a normalized vector from the center of rigid body i in the direction of the patch, which depends on $\mathbf{\Omega}_i$, and cos θ_{ijp_i} is the scalar product of the normalized vector $\hat{\mathbf{r}}_{ij}$ with $\mathbf{p}_i$. The width of the patches is controlled by the parameter cos δ. The chosen forms of eqs 5 and 7 make the respective functions and their first derivatives continuous (Figure 1). We employed an angle-axis representation for rigid-body rotational coordinates,[45,46] and analytical first derivatives were obtained in a computationally efficient way.[46]

For computational accuracy under periodic boundary conditions, it is useful to have V decreasing continuously to zero at some cutoff distance less than half the smallest cell dimension. To achieve this functional form, a modified version of U_{M} was used:[47]

$$U_{\mathrm{M}}^{\mathrm{per}}(r_{ij}) = 4\left\{\left[\left(\frac{\sigma}{r_{ij}}\right)^{46} - \left(\frac{\sigma}{r_{ij}}\right)^{23}\right] + \left[23\left(\frac{\sigma}{r_c}\right)^{46} - \frac{23}{2}\left(\frac{\sigma}{r_c}\right)^{23}\right]\left(\frac{r_{ij}}{r_c}\right)^2 - 24\left(\frac{\sigma}{r_c}\right)^{46} + \frac{25}{2}\left(\frac{\sigma}{r_c}\right)^{23}\right\} \quad (8)$$

where r_c is the cutoff distance, beyond which $U_{\mathrm{M}}^{\mathrm{per}} = 0$. This form has first derivatives that also go continuously to zero at r_c. No adjustment to the PAP interaction is required, as long as $\lambda + s^{-1} < r_c$, as the PAP interaction already tends to zero. The modified form does not differ significantly in the well region from eq 3 for $r_c > 2.5$. Therefore the length of the cubic box was set greater than 5.

Structure Prediction. For structure prediction we employed the basin-hopping (BH) global optimization technique,[48−50] as implemented in the program GMIN,[51] which uses a customized L-BFGS minimizer[52] to reduce the total root-mean-square (RMS) force to a specified tolerance for each proposed step. Typically we employed 10^5 BH steps, each involving random particle displacements in both translational and rotational coordinates, starting from 10 random configurations. The step sizes are much larger than those commonly used in Monte Carlo simulations of equilibrium thermodynamics, since the objective here is to step out of a basin. If these runs produced a consensus for the lowest minimum, this structure was accepted as the putative global minimum. Otherwise, longer BH runs were conducted until this condition was achieved. In some cases a Bernal spiral, identified as a putative global minimum for a different set of parameters, was used as the starting configuration to check the convergence.

Percolation. The standard method in GMIN to prevent particles evaporating from a finite-sized cluster is to contain them within a sphere. Any particles that move outside the spherical container during a BH step or minimization are replaced within the sphere. It seemed likely that, for the short-ranged PAP potential, and considering the anisotropic morphology of the Bernal spiral, this method might not be optimal. An alternative approach is to require that any potential minimum is a percolating structure, meaning that it is possible to find a path from any one particle to any other particle by steps between particles no larger than a certain defined distance. In the language of graph theory, if a graph is formed with particles as the vertices, and an edge added between any two particles less than the cutoff distance from each other, the graph is required to be connected.[53] The connectivity of the graph can be assessed efficiently with a depth-first search.[54] Additionally, a harmonic compression potential, with a specified force constant, was used to help produce connected clusters, and was turned off when a chosen RMS force was achieved in each minimization. BH steps and minimizations were performed until a percolating minimum was found. Thereafter, any step that produced a disconnected minimum was rejected. For the relatively small systems considered in the present work, both the percolation condition and a spherical container proved to be effective.

Monte Carlo Simulations. We performed Monte Carlo simulations in the NVT ensemble for a system of $N = 300$ particles

enclosed in a cubic box at a packing fraction of $\phi = \pi/6\rho d^3 = 0.0058$. After equilibration at a high temperature ($T = 1.0$), the system was quenched instantaneously to a series of temperatures of interest. Following equilibration, simulations were run for 10^7 MC steps. Each MC step consisted of N attempts for single-particle translational and rotational moves each.[15]

Conflict of Interest: The authors declare no competing financial interest.

Acknowledgment. We are very grateful to Prof. Daan Frenkel for helpful discussions and acknowledge support from ERC grant 267369 and EPSRC Programme grant EP/I001352/1. D.C. acknowledges support *via* a Ramanujan Fellowship from the Department of Science and Technology, Govt. of India. N.D. acknowledges support from the Swiss National Science Foundation (Project No. PBELP2-130895).

REFERENCES AND NOTES

1. Parak, W. J. Complex Colloidal Assembly. *Science* **2011**, *334*, 1359–1360.
2. Edwards, E. W.; Wang, D.; Möhwald, H. Hierarchical Organization of Colloidal Particles: From Colloidal Crystallization to Supraparticle Chemistry. *Macromol. Chem. Phys.* **2007**, *208*, 439–445.
3. Glotzer, S. C.; Solomon, M. J. Anisotropy of Building Blocks and their Assembly into Complex Structures. *Nat. Mater.* **2007**, *6*, 557–562.
4. Yang, S.-M.; Kim, S.-H.; Lim, J.-M.; Yi, G.-R. Synthesis and Assembly of Structured Colloidal Particles. *J. Mater. Chem.* **2008**, *18*, 2177–2190.
5. Calvo, F.; Doye, J. P. K.; Wales, D. J. Energy Landscapes of Colloidal Clusters: Thermodynamics and Rearrangement Mechanisms. *Nanoscale* **2012**, *4*, 1085–1100.
6. Wales, D. J. *Energy landscapes*; Cambridge University Press: Cambridge, UK, 2003.
7. Wales, D. J. Energy Landscapes: Calculating Pathways and Rates. *Int. Rev. Phys. Chem.* **2006**, *25*, 237–282.
8. Wales, D. J.; Doye, J. P. K.; Miller, M. A.; Mortenson, P. N.; Walsh, T. R. Energy Landscapes: From Clusters to Biomolecules. *Adv. Chem. Phys.* **2000**, *115*, 1.
9. Noro, M. G.; Frenkel, D. Extended Corresponding-States Behavior for Particles with Variable Range Attractions. *J. Chem. Phys.* **2000**, *113*, 2941–2944.
10. Malins, A.; Williams, S. R.; Eggers, J.; Tanaka, H.; Royall, C. P. Geometric Frustration in Small Colloidal Clusters. *J. Phys.: Condens. Matter* **2009**, *21*, 425103.
11. Vliegenthart, G. A.; Lekkerkerker, H. N. W. Predicting the Gas–Liquid Critical Point from the Second Virial Coefficient. *J. Chem. Phys.* **2000**, *112*, 5364–5369.
12. Taffs, J.; Malins, A.; Williams, S. R.; Royall, C. P. A Structural Comparison of Models of Colloid–Polymer Mixtures. *J. Phys.: Condens. Matter* **2010**, *22*, 104119.
13. Wales, D. J. Highlights: Energy Landscapes of Clusters Bound by Short-Ranged Potentials. *ChemPhysChem* **2010**, *11*, 2491–2494.
14. Pawar, A. B.; Kretzschmar, I. Fabrication, Assembly, and Application of Patchy Particles. *Macromol. Rapid Commun.* **2010**, *31*, 150–168.
15. Kern, N.; Frenkel, D. Fluid–Fluid Coexistence in Colloidal Systems with Short-Ranged Strongly Directional Attraction. *J. Chem. Phys.* **2003**, *118*, 9882–9889.
16. Zhang, Z.; Glotzer, S. C. Self-Assembly of Patchy Particles. *Nano Lett.* **2004**, *4*, 1407–1413.
17. Wilber, A. W.; Doye, J. P. K.; Louis, A. A. Self-Assembly of Monodisperse Clusters: Dependence on Target Geometry. *J. Chem. Phys.* **2009**, *131*, 175101.
18. Almarza, N. G.; Noya, E. G. Phase Transitions of a Lattice Model for Patchy Particles with Tetrahedral Symmetry. *Mol. Phys.* **2011**, *109*, 65–74.
19. Ngo, T. T.; Liddell, C. M.; Ghebrebrhan, M.; Joannopoulos, J. D. Tetrastack: Colloidal Diamond-Inspired Structure with Omnidirectional Photonic Band Gap for Low Refractive Index Contrast. *Appl. Phys. Lett.* **2006**, *88*, 241920.
20. Romano, F.; Sanz, E.; Sciortino, F. Crystallization of Tetrahedral Patchy Particles *in Silico*. *J. Chem. Phys.* **2011**, *134*, 174502.
21. Yang, S.; Cho, S. S.; Levy, Y.; Cheung, M. S.; Levine, H.; Wolynes, P. G.; Onuchic, J. N. Domain Swapping is a Consequence of Minimal Frustration. *Proc. Natl. Acad. Sci. U.S.A.* **2004**, *101*, 13786–13791.
22. Doye, J. P. K.; Louis, A. A.; Lin, I.-C.; Allen, L. R.; Noya, E. G.; Wilber, A. W.; Kok, H. C.; Lyus, R. Controlling Crystallization and its Absence: Proteins Colloids and Patchy Models. *Phys. Chem. Chem. Phys.* **2007**, *9*, 2197–2205.
23. Hloucha, M.; Lodge, J.; Lenhoff, A.; Sandler, S. A Patch–Antipatch Representation of Specific Protein Interactions. *J. Cryst. Growth* **2001**, *232*, 195–203.
24. Dorsaz, N.; Filion, L.; Smallenburg, F.; Frenkel, D. Effect of Interaction Specificity on the Phase Behaviour of Patch Particles. *Faraday Discuss.* **2012**, *159*, 9–2110.1039/C2FD20070H.
25. Bernal, J. D. The Bakerian Lecture, 1962. The Structure of Liquids. *Proc. R. Soc. London, A* **1964**, *280*, 299–322.
26. Deer, W. A.; Howie, R. A.; Sussman, J. *An Introduction to the Rock-Forming Minerals*, 2nd ed.; Prentice Hall: Upper Saddle River, NJ, 1992.
27. Bronger, W.; Gunther, O. Darstellung und Struktur von K_2PtS_2 und Rb_2PtS_2. *J. Less-Common Met.* **1972**, *27*, 73–79.
28. Zheng, C.; Hoffmann, R.; Nelson, D. R. A Helical Face-Sharing Tetrahedron Chain from Irrational Twist, Stella Quadrangula, and Related Matters. *J. Am. Chem. Soc.* **1990**, *112*, 3784–3791.
29. Steinhardt, P. J.; Nelson, D. R.; Ronchetti, M. Bond-Orientational Order in Liquids and Glasses. *Phys. Rev. B* **1983**, *28*, 784–805.
30. Nelson, D. R. Order, Frustration, and Defects in Liquids and Glasses. *Phys. Rev. B* **1983**, *28*, 5515–5535.
31. Campbell, A. I.; Anderson, V. J.; van Duijneveldt, J. S.; Bartlett, P. Dynamical Arrest in Attractive Colloids: The Effect of Long-Range Repulsion. *Phys. Rev. Lett.* **2005**, *94*, 208301.
32. Liu, Y.; Porcar, L.; Chen, J.; Chen, W.-R.; Falus, P.; Faraone, A.; Fratini, E.; Hong, K.; Baglioni, P. Lysozyme Protein Solution with an Intermediate Range Order Structure. *J. Phys. Chem. B* **2011**, *115*, 7238–7247.
33. Chen, Q.; Whitmer, J. K.; Jiang, S.; Bae, S. C.; Luijten, E.; Granick, S. Supracolloidal Reaction Kinetics of Janus Spheres. *Science* **2011**, *331*, 199–202.
34. Sciortino, F.; Tartaglia, P.; Zaccarelli, E. One-Dimensional Cluster Growth and Branching Gels in Colloidal Systems with Short-Range Depletion Attraction and Screened Electrostatic Repulsion. *J. Phys. Chem. B* **2005**, *109*, 21942–21953.
35. Toledano, J. C. F.; Sciortino, F.; Zaccarelli, E. Colloidal Systems with Competing Interactions: From an Arrested Repulsive Cluster Phase to a Gel. *Soft Matter* **2009**, *5*, 2390–2398.
36. Pacheco-Contreras, R.; Dessens-Félix, M.; Borbón-González, D. J.; Paz-Borbón, L. O.; Johnston, R. L.; Schön, J. C.; Posada-Amarillas, A. Tetrahelix Conformations and Transformation Pathways in Pt1Pd12 Clusters. *J. Phys. Chem. A* **2012**, *116*, 5235–5239.
37. Wales, D. J.; Doye, J. P. K.; Dullweber, A.; Hodges, M. P.; Naumkin, F. Y.; Calvo, F.; Hernández-Rojas, J.; Middleton, T. F. The Cambridge Cluster Database http://www-wales.ch.cam.ac.uk/CCD.html, 2012.
38. Doye, J. P. K.; Wales, D. J. The Structure and Stability of Atomic Liquids: From Clusters to Bulk. *Science* **1996**, *271*, 484–487.
39. Doye, J. P. K.; Wales, D. J. The Effect of the Range of the Potential on the Structure and Stability of Simple Liquids: From Clusters to Bulk, from Sodium to C_{60}. *J. Phys. B* **1996**, *29*, 4859–4894.
40. Romano, F.; Sciortino, F. Patterning Symmetry in the Rational Design of Colloidal Crystals. *Nat. Commun.* **2012**, *3*, 975.
41. Pellegrini, M.; Wukovitz, S. W.; Yeates, T. O. Simulation of Protein Crystal Nucleation. *Proteins* **1997**, *28*, 515–521.

42. Liu, H.; Kumar, S. K.; Douglas, J. F. Self-Assembly-Induced Protein Crystallization. *Phys. Rev. Lett.* **2009**, *103*, 018101.
43. Mie, G. Zur Kinetischen Theorie der Einatomigen Körper. *Ann. Phys., Berlin* **1903**, *316*, 657–697.
44. ten Wolde, P. R.; Frenkel, D. Enhancement of Protein Crystal Nucleation by Critical Density Fluctuations. *Science* **1997**, *277*, 1975–1978.
45. Wales, D. J. The Energy Landscape as a Unifying Theme in Molecular Science. *Phil. Trans. Roy. Soc. A* **2005**, *363*, 357–377.
46. Chakrabarti, D.; Wales, D. J. Simulations of Rigid Bodies in an Angle-Axis Framework. *Phys. Chem. Chem. Phys.* **2009**, *11*, 1970–1976.
47. Stoddard, S. D.; Ford, J. Numerical Experiments on the Stochastic Behaviour of a Lennard-Jones Gas System. *Phys. Rev. A* **1973**, *8*, 1504–1512.
48. Li, Z.; Scheraga, H. A. Monte Carlo-Minimization Approach to the Multiple-Minima Problem in Protein Folding. *Proc. Natl. Acad. Sci. U.S.A.* **1987**, *84*, 6611–6615.
49. Wales, D. J.; Doye, J. P. K. Global Optimization by Basin-Hopping and the Lowest Energy Structures of Lennard-Jones Clusters Containing up to 110 Atoms. *J. Phys. Chem. A* **1997**, *101*, 5111–5116.
50. Wales, D. J.; Scheraga, H. A. Global Optimization of Clusters, Crystals, and Biomolecules. *Science* **1999**, *285*, 1368–1372.
51. Wales, D. J. GMIN: A Program for Basin-Hopping Global Optimisation http://www-wales.ch.cam.ac.uk/GMIN/, 2012.
52. Nocedal, J. Updating Quasi-Newton Matrices with Limited Storage. *Math. Comput.* **1980**, *35*, 773–782.
53. Diestel, R. *Graph Theory*, 4th ed.; Springer: Heidelberg, 2010.
54. Even, S. *Graph Algorithms*, 2nd ed.; Cambridge University Press: Cambridge, UK, 2011.